59th Electric Furnace and 19th Process Technology Conferences, Phoenix Civic Plaza Convention Center, Phoenix AZ, 11-14 November 2001

GRAIN REFINEMENT OF FULLY AUSTENITIC STAINLESS STEELS USING A Fe-Cr-Si-Ce MASTER ALLOY

Casper van der Eijk and John Walmsley
SINTEF Materials Technology
N-7465 Trondheim, Norway
+47-98283989
casper.eijk@sintef.no

Øystein Grong
Norwegian University of Science and Technology
Department of Materials Technology and Electrochemistry
N-7491 Trondheim, Norway

Ole Svein Klevan
Elkem ASA
N-7301 Orkanger, Norway

Key Words: Stainless Steel, Grain Refinement, Inclusions, Rare Earth Metals, Ferroalloys

INTRODUCTION

Grain size control is one of the most important aspects in the processing of metals and alloys. This is due to the fact that most engineering properties are strongly influenced by the grain size. The best examples are yield strength, as represented by the Hall-Petch relationship, and toughness, which both benefit from a small grain size. In addition, steel processing also benefits from a small grain size, since centerline or interdendritic segregation can be reduced, and hence, problems with high temperature cracking can be minimized.

In recent years, a number of investigations have been made on the use of rare-earth metal additions to steel in view of their ability to modify the solidification structure. Several studies have shown that the dendritic solidification structure is refined because new primary dendritic arms are generated near the liquid-solid interface due some unsettled effects caused by REM addition. However, undercooling measurements have confirmed that REM-oxides can act as effective nucleants to refine the as-cast structure of iron[1-8]. The goal of the present work is to investigate the effect of such seed crystals by generating deoxidation products in the liquid steel through the addition of a so-called “preconditioner”, which under the prevailing circumstances act as a grain refiner.

EXPERIMENTAL

Two different batches of 254 SMO were investigated. 254 SMO is a "superaustenitic" stainless steel with the nominal composition 20 Cr-18 Ni-6 Mo. It has high strength and good resistance to chloride pitting, crevice corrosion and stress corrosion cracking. As fully austenitic steels do not undergo a phase transformation in the solid state, there is particularly a need of grain refining in this case.

Alloy composition

A Fe-Cr based ferroalloy for use in stainless steel was produced at Elkem Research in Kristiansand. The purpose of the alloy is to transform oxide inclusions in the steel to inclusions which have grain refining capabilities. The analyzed composition of the alloy is shown in Table I. The purpose of the Si addition is to decrease the melting temperature of the alloy.

Table I The composition of the Fe-Cr based preconditioner (wt.%).

Cr	Si	Ce	C	Fe
32.0	17.6	8.7	1.24	balance

Two heats of 254 SMO, each consisting of about 5 tons of liquid steel, were prepared in an AOD converter at Scana Steel Stavanger. After transfer to the tapping ladle, the melt temperature was about 1495°C. In the reference casting, solid rods of mischmetal were added to the liquid steel in the tapping ladle. This is normal practice for these steels at Scana Steel Stavanger. In the experimental casting, 3.5 kg of the preconditioner was added per ton of liquid steel in the tapping ladle as the final preconditioning step in replacement of the mischmetal additions. The target Ce content was 0.03 wt%. Shortly thereafter the steel was cast in an iron mould, using a conventional assembly for bottom pouring. The total weight of the ingot was 3.4 tons. Table II shows the composition of the alloys. The Ce content in the experimental steel is only 0.01wt%. The main differences between the compositions of the two steel are the oxygen content, which is unintentionally higher in the experimental steel, and the La content, which is essentially zero in the experimental steel, while present in the reference steel through the mischmetal additions.

Specimen preparation

Figures 1 and 2 show a sketch of the ingot cast at Scana Steel Stavanger and the positions from which the specimens for metallographic and TEM investigations were taken. Metallographic specimens were prepared according to standard techniques and finally etched using Vilella's reagent. The non-metallic inclusions, present in the steels as a result of deoxidation practice, were investigated in TEM and a Jeol-8900 microprobe equipped with both EDS and WDS detectors.

Table II Chemical composition of the different 254 SMO alloys examined (wt%).

wt%	Reference casting, treated with mischmetal	Experimental casting, treated with Ce-containg preconditioner
C	0.03	0.022
Si	0.54	0.39
Mn	0.49	0.58
P	0.022	0.025
S	0.001	0.001
Cr	20.1	20.2
Ni	17.6	17.7
Al	0.01	0.01
Cu	0.7	0.75
Mo	6.2	6.1
Nb	0.02	0.02
V	0.08	0.08
Ti	0.01	0.01
Co	0.07	0.11
B	0.002	0.001
W	0.15	0.15
Sn	0.006	0.006
N	0.19	0.21
Ce	0.01	0.01
O	0.005	0.01
La	0.005	0.00

The TEM/STEM inclusion analyses were carried out using a Philips CM 30 transmission electron microscope equipped with an EDS unit for element analyses. A special preparation procedure was employed to achieve transparent foils with the inclusions embedded in the steel matrix. Large (>1μm) oxide inclusions are difficult to prepare by electropolishing or ion beam thinning at large angles (>~5^{o}). Here, 3mm diameter discs of steel were mechanically ground to ~80μm thickness and dimple ground to a central thickness of ~30μm. The ion-beam thinning is performed at an angle of <3.5° in a Gatan PIPS system. The sample was thinned from both sides until perforated. At the low thinning angle, the inclusions are protected from the ion beam by the matrix. The foil can be observed in the optical microscope without being removed from the mount. Under reflected light, the grain structure around the inclusions is sometimes visible. A suitable inclusion close to the perforation is selected. The sample is then turned over and ion-thinned from one side only until the same inclusion is seen from the second side of the sample. Under transmitted light, the oxide phases become transparent when the sample is around 1 micrometer thick. Final thinning is done in several stages and monitored by examining the sample in the TEM. Although significant thickness variations were still present, the composition of the inclusion constituent phases can be measured with high spatial resolution by EDS and X-ray imaging. The crystal structure and orientation of the phases are determined by Selected Area Electron Diffraction (SAD).

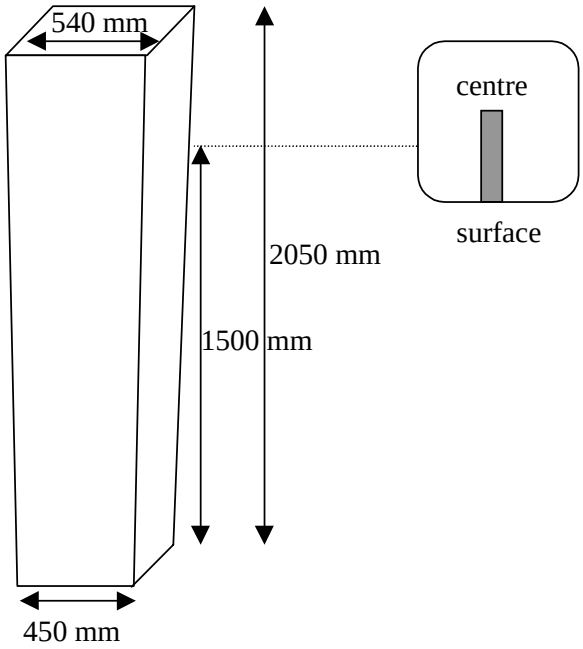

Fig. 1: Sketch showing the dimensions of the cast ingot. The location of the bar taken out for microstructure examination is also indicated.

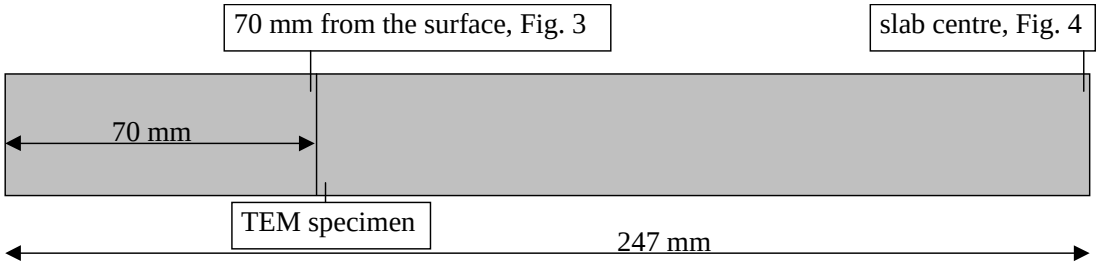

Fig. 2: Sketch of the bar taken from the ingot position indicated in Fig. 1 showing the positions from which the specimens for metallographic and TEM investigations are taken.

RESULTS AND DISCUSSION

Solidification microstructure

Metallographic examination reveals large differences in the microstructure of the two steels. In Fig. 3, the austenite grain boundaries are visible as weak solid lines in the micrographs. More notable, is the observed difference in the dendritic morphology, which is significantly finer in the experimental steel treated with the Ce-containing preconditioner compared with the reference casting. At this position, the dendrite arm spacing differs roughly by a factor of three. The situation is quite similar towards the center of the casting, as shown in Fig. 4, although a general coarsening of the microstructure has occurred. At this position the dendrite arm spacing differs by a factor of about two in favor of the experimental casting. Note that the dark spots observed in the micrographs reflect micro (shrinkage) porosity.

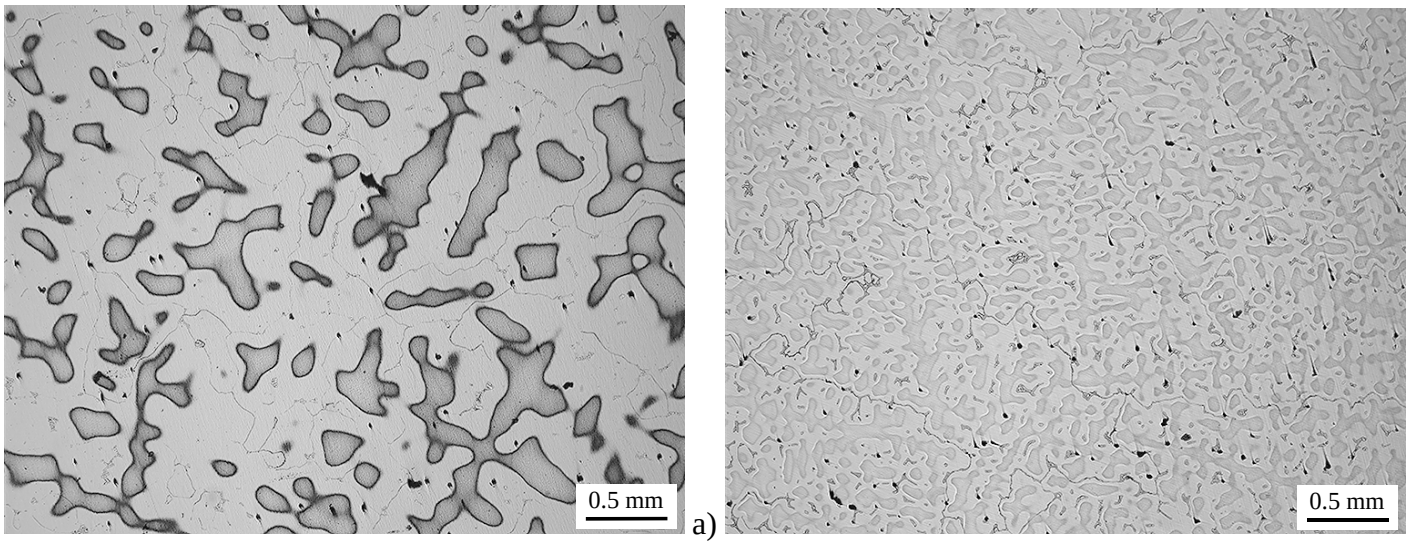

Fig. 3: Microstructure of a) the reference steel and b) the experimental steel treated with the Ce-containing preconditioner, 70 mm from the ingot surface.

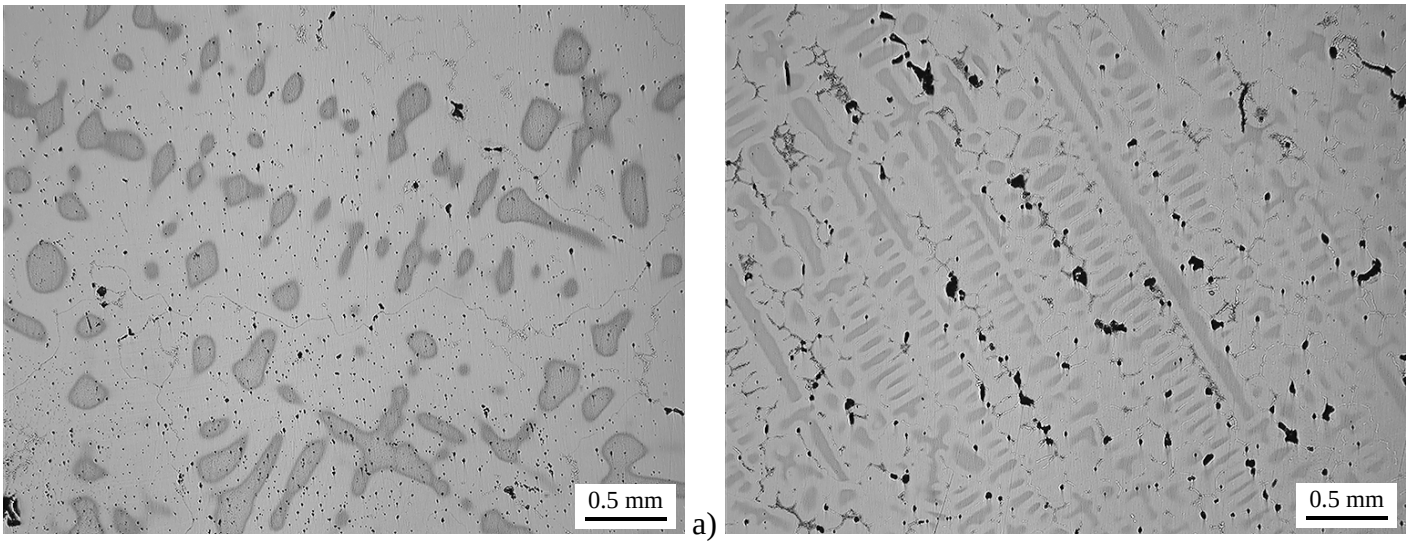

Fig. 4: Microstructure of a) the reference steel and b) the experimental steel treated with the Ce-containing preconditioner, in the center of the ingot.

Inclusion characterization

Quantitative characterization of the inclusions in the steels in the optical microscope shows that the average size of the inclusions is 2.3 μm and 3.1 μm, while the inclusion number density is $6.8x10^{13}/m^3$ and $2.4x10^{13}/m^3$ for the reference and experimental steel, respectively.

The average chemical composition of the inclusions is shown in Table III. The compositional variations between the inclusions are small.

Table III Average chemical composition of five inclusions, using WDS microprobe analyses (at%).

	Al	Ce	La	O	Si	Mn	Ti	S
Reference steel	1.6±1.1	23.4±2.3	8.6±1.4	64.6±0.8	0.7±0.4	0.3±0.3	0.4±0.4	0.3±0.2
Experimental steel	9.4±2.3	25.0±2.2	0.0±0.0	60.6±1.0	3.3±0.4	0.6±0.4	0.0±0.0	1.1±1.1

The X-ray mapping done in the TEM showed that the inclusions studied consisted mainly of one phase. For the reference material La and Ce were found to co-exist in the same oxide. These two elements are difficult to distinguish in EDS maps because their *L* edge peaks overlap. EDS of single crystal particles in the experimental steel showed the presence of Ce and Al. Phase identification was performed by recording several diffraction patterns from different samples of the main oxide phase in both the reference steel and the experimental steel.

Figure 5a shows a TEM micrograph of an inclusion in the reference steel. Diffraction patterns consistent with the cubic $Ce_{0.73}La_{0.27}O_{1.87}$ phase (space group Fm3m) were obtained, Figure 5b[9]. From the EDS results and the EPMA results shown in Table III, there is clearly substitution of Ce by La in the structure.

For the inclusions in the experimental steel, diffraction patterns consistent with the $CeAlO_3$ phase were obtained, Figure 6. This is a tetragonal perovskite structure, although the distortion from the ideal cubic structure is probably too small to distinguish in the diffraction patterns[10]. The inclusion shown in Figure 6 is a single crystal oxide, containing some discrete Mg impurity. In some cases the inclusions could also contain patches of MoC at the surface (not shown here).

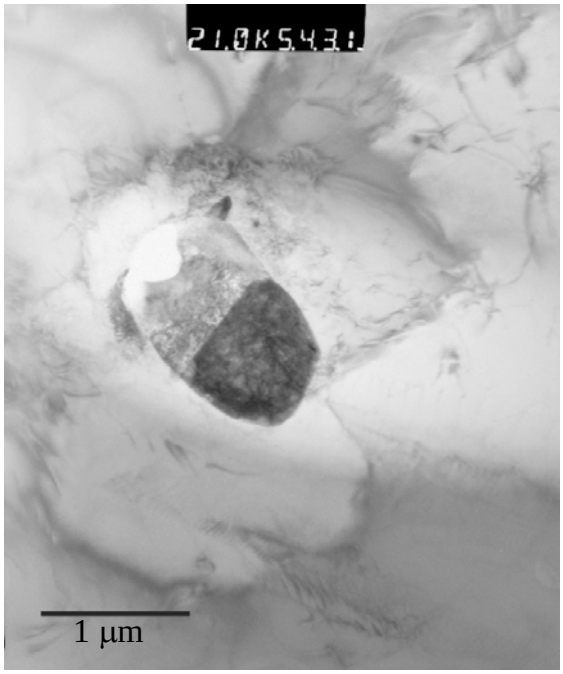

a)

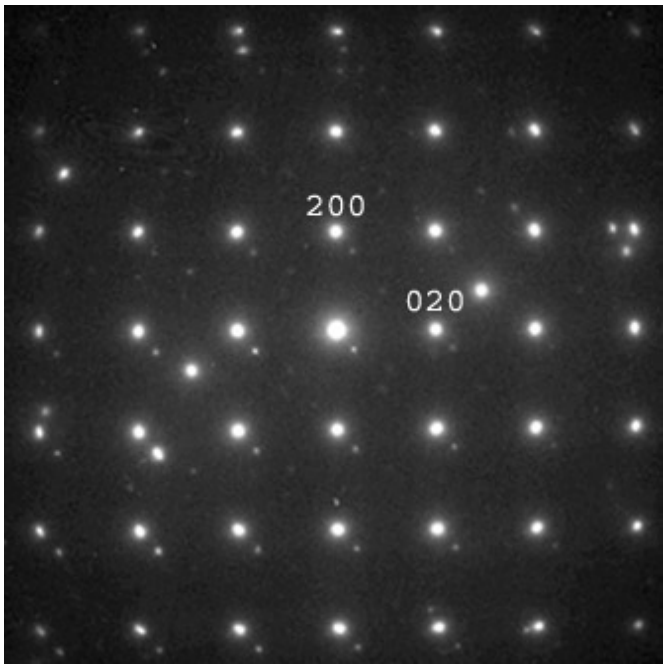

b)

Fig. 5: a) TEM micrograph of an inclusion in the reference steel and b) indexed diffraction pattern.

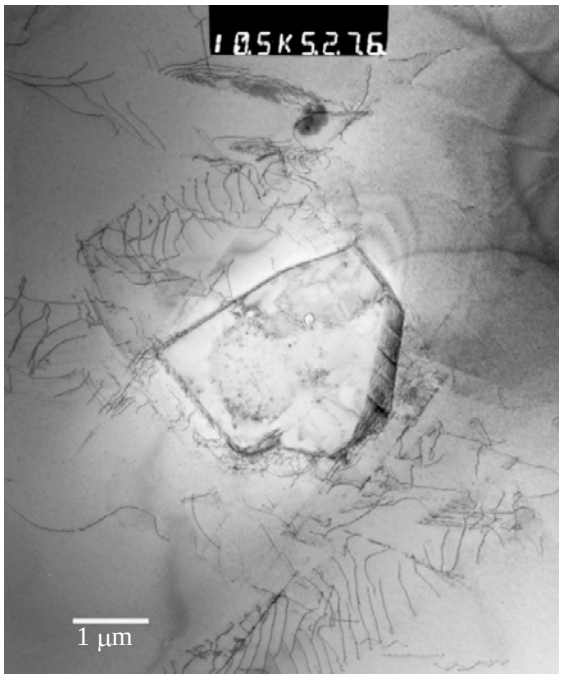

a)

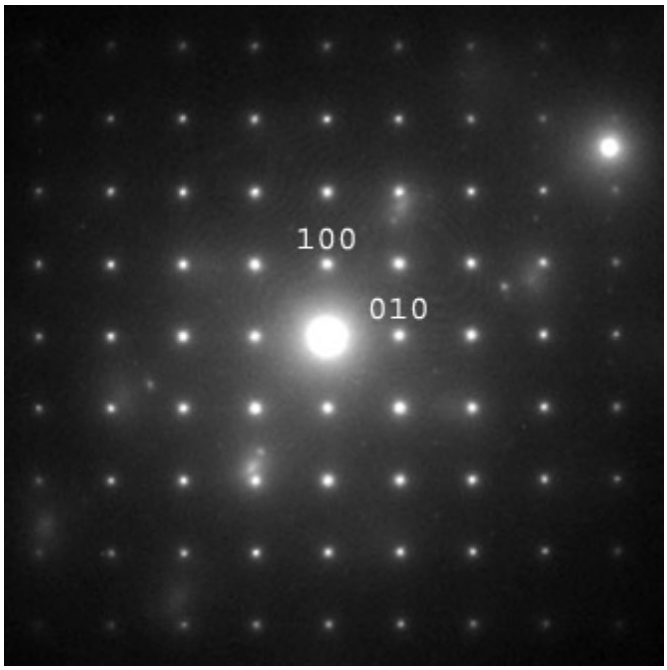

b)

Fig. 6: a) TEM micrograph of an inclusion in the experimental steel and b) indexed diffraction pattern.

The mechanism of heterogeneous nucleation by REM-oxides

If inclusions are formed prior to solidification and thus are solid when the metal is freezing, they can possibly act as effective heterogeneous nucleation sites during solidification. Rare earth metals are strong oxideformers. Thermodynamic calculations on the stability of Ce- and La-oxides in liquid steel by means of the Thermo-Calc computer programme indicate that these compounds are present prior to solidification.

The balance of interfacial energies between the nucleant, nucleus and the liquid metal is the controlling factor in heterogeneous nucleation. But experimental data on solid/liquid interfacial energies is scarce and not very reliable. In addition, a simple description of the interfacial energy is difficult since the total interfacial free energy of the system is composed of several contributing factors. These factors include, the chemical nature of the substrate, the topographic features of the substrate surface, the electrostatic potential between the substrate and the nucleated solid, and the degree of atomic misfit or lattice disregistry between the two phases at the interface. The latter can be calculated on the basis of the Bramfitt's planar lattice disregistry model [11]:

$$\delta^{(hkl)_s}_{(hkl)_n} = \sum_{i=1}^{3} \frac{1}{3} \left(\frac{\left| (d_{[uvw]_s^i} \cos\gamma) - d_{[uvw]_n^i} \right|}{d_{[uvw]_n^i}} \right) \text{x}100\% \qquad (1)$$

where, $(hkl)_s$ = a low-index plane of the substrate;

$[uvw]_s$ = a low-index direction in $(hkl)_s$;

$(hkl)_n$ = a low-index plane in the nucleated solid;

$[uvw]_n$ = a low-index direction in $(hkl)_n$;

$d_{[uvw]_n}$ = the interatomic spacing along $[uvw]_n$;

$d_{[uvw]_s}$ = the interatomic spacing along $[uvw]_s$;

γ = the angle between the $[uvw]_s$ and the $[uvw]_n$.

One can now in principle calculate the lattice disregistry between the austenite phase and the observed oxide phases. There is however uncertainty in the lattice parameters of the oxides at solidification temperature, since the dilatation parameters of the oxide phases are not known. An estimate of the lattice disregistry at 1773K is given in Table IV. For these calculations the values at room temperature were used and extrapolated using assumed dilatation coefficients. The $AlCeO_3$ appears to have the smallest lattice disregistry with the solidifying austenite phase. This could explain the significantly finer solidification microstructure of the experimental steel.

Table IV Lattice disregistry between austenite and the observed oxides at 1500K.

	Lattice constant /nm (293 K)	Linear dilatation $x10^{-6}$/K	Lattice constant /nm (1773 K)	Lattice disregistry	Orientation
Austenite	0.356 [2]	23	0.368		
$AlCeO_3$	0.3767 (a) [10]	10*	0.382	3.82%	$(100)_\gamma//(100)_{AlCeO3}$ $[100]_\gamma//[100]_{AlCeO3}$
	0.3797 (c) [10]	10*	0.385	4.65%	$(100)_\gamma//(001)_{AlCeO3}$ $[100]_\gamma//[001]_{AlCeO3}$
$Ce_{0.73}La_{0.27}O_{1.87}$	0.549 [9]	10*	0.557	6.26%	$(100)_\gamma//(111)_{CeLaO2}$ $[001]_\gamma//[110]_{CeLaO2}$

* estimated value

SUMMARY

Two different batches of S254-SMO austenitic stainless steels have been produced, one with addition of mischmetal (Ce+La), and one with addition of Ce only via a Fe-Cr-Si-Ce master alloy. Metallographic examination reveals that a substantial reduction in the dendrite arm spacing can be achieved in the latter case by promoting the formation of Ce-Al-oxide inclusions in the liquid steel prior to solidification, which have a good crystallographic compatibility with the austenite.

ACKNOWLEDGEMENTS

The authors would like to acknowledge the Norwegian Research Council and the Norwegian Ferroalloy Producers Research Association for the financial support and also wish to thank Hilde Marit Skauge and Morten Langøy from Scana Steel Stavanger for their co-operation to the project.

REFERENCES

1. J. Lan, J. He, W. Ding, Q. Wang and Y. Zhu, “Effect of Rare Earth Metals on the Microstructure and Impact Toughness of a Cast 0.4C-5Cr-1.2Mo-1.0V Steel”, ISIJ Int., Vol. 40, 2000, No. 12, pages 1275-1282.

2. Q. Yang, X. Ren, B. Liao, M. Yao and X. Wan, “Discussion of RE Inclusions as Heterogeneous Nuclei of Primary Austenite in Hardfacing Metals of Medium-High Carbon Steels”, Journal of Rare Earths, Vol. 17, 1999, No. 4, pages 293-297.

3. P.E. Waudby, “Rare Earth Additions to Steel”, Int. Mat. Rev., Vol. 229, 1978, No. 2, pages 74-99.

4. M. Guo and H. Suito, “Influence of Dissolved Cerium and Primary Inclusion Particles of Ce2O3 and CeS on Solidification Behavior of Fe-0.20 mass% C- 0.02 mass% P Alloy”, ISIJ int., Vol. 39, 1999, No. 7, pages 722-729.

5. J.J. Moore, “Modification of the Cast Structure Using Rare Earth Additions.”, AIME Steelmaking Porc., Vol. 67, 1984, pages 239-254.

6. Y. Nuri, T. Ohashi, T. Hiromoto and K. Kitamura, “Solidification Microstructure of Ingots and Continuously Cast Slabs Treated with Rare Earth Metal.”, Trans. ISIJ, Vol. 22, 1982, pages 399-407.

7. Y. Nuri, T. Ohashi, T. Hiromoto and K. Kitamura, “Solidification Macrostructure of Ingots and Continuously Cast Slabs Treated with Rare Earth Metal.”, Trans. ISIJ, Vol. 22, 1982, pages 408-416.

8. H. Li, A. McLean, J.W. Rutter and I.D. Sommerville, “Influence of Rare Earth Metals on the Nucleation and Solidification Behavior of Iron and 1045 Steel”, Metall. Trans. B, Vol. 19B, 1988, pages 383-395.

9. B.C. Morris, W.R. Flavell, W.C. Mackrodt and M.A. Morris, “Lattice Parameter Changes in the Mixed-oxide System $Ce_{1-x}La_xO_{2-x/2}$: A Combined Experimental and Theoretical Study”, J. Mater. Chem., Vol. 3, 1993, pages 1007-1013.

10. M. Tanaka, T. Shishido, H. Horiuchi, N. Toyota, D. Shindo and T. Fukuda, “Structure studies of $CeAlO_3$”, Journal of Alloys and Compounds, Vol. 192, 1993, pages 87-89.

11. B.L. Bramfitt, “The Effect of Carbide and Nitride Additions on the Heterogeneous Nucleation Behavior of Liquid Iron.”, Metall. Trans., Vol. 1, 1970, pages 1987-1995.